Investigating the Almost Featureless Spectrum of the Radio-Quiet AGN: BL Lacertae

Zachary Stone[1]
Stony Brook University, Stony Brook, NY 11793
zachary.stone@stonybrook.edu

ABSTRACT

This is an analysis of data for spectra of the famously known active galactic nucleus BL Lacertae. Most of the features on the spectrum will be severely Doppler broadened due to the high velocities of the material in the jet of the blazar. The main purpose of this paper, and the data analysis involved within it, will be to determine the spectral features of BL Lac, calculate its redshift, and determine the properties of the material within BL Lac. Doing so, I will touch upon the differences between different classes of BL Lac objects, as well as the issue pertaining to the different types of emission lines seen in their spectra. Using certain methods from Python in the `scipy` package, I then fit for the characteristic of each observed extremum in the spectrum, and determine their characteristics. After filtering certain spectral lines, I then fit for various redshifts of various spectral line transitions, and determine the best possible value for the redshift of BL Lacertae. After various reduction techniques, I find that the spectrum of BL Lac contains highly relativistic Hydrogen, in Hβ emission, relativistic, ionized Helium, in He-I absorption, and O-III within the host galaxy. These spectral lines contain information about the classification of BL Lac as a blazar, and help characterize the material within the medium surrounding the galaxy. Further analysis on these features can be used to determine characteristics of the host galaxy, the mechanisms creating the jet, feedback within the galaxy, and dynamics of its central black hole.

Subject headings: active galactic nuclei, AGN, BL Lac, emission/absorption lines

1. Introduction

Active galactic nuclei (AGN) are highly luminous extragalactic point sources. Initially thought of as variable stars, these bright sources of, in many cases, highly redshifted light all stem from the center of a galaxy. The ways in which this light from active galactic nuclei can vary due to the mechanisms producing the light. In most cases, this light is being produced from a black hole in the center of the galaxy, either by matter accreting onto the black hole, or a jet stemming from the center of the black hole. As the gravity draws the infalling material closer and closer, the density of material near the black hole becomes higher and higher. Furthermore, angular momentum is conserved as these particles creep closer to the galactic center, imbuing them with high, many times relativistic speeds. These particles with then collide with each other or release energy in a thermal fashion, which can be seen from millions of parsecs. This accretion of matter onto the black hole can be disturbed from various properties within the galaxy, including the composition of material within the accretion disk, the rate of accretion, and turbulence within the accretion disk.

The other mechanism which produces light in an active galactic nucleus is a jet which would stem from its center, funneling material outward into the intergalactic or circumgalactic medium (IGM/CGM). A subcategory of AGN are labeled blazars, which are all angled along our line of sight

[1]Main (and only) author and contributor

when viewing them. Normally, an AGN can be angled in any arbitrary direction, meaning we would see the jet coming out from the side, or less accretion disk radiation. When looking down the center of the AGN, especially if a jet is involved, most of the radiation we see is from relativistic particles. In many cases, these particles seem to be moving at superluminal speeds. This causes the radiation we see to be highly redshifted as well, meaning traveling at a much higher speed then the rest of the galaxy, or other particles within the galaxy. The fact that we are looking "down the barrel" of the AGN, also means that the radiation seen from the galaxy will be very variable, in terms of its polarization and intensity. The radiation can change rapidly depending on the mechanism producing the jet, the material within the accretion disk, and the rate of accretion.

This radiation from the AGN can also be considered radio-loud or radio-quiet. One class of blazars is named flat-radio spectrum quasars (FSRQs), which are radio-loud. The spectra of these objects exhibit mild, or even strong, absorption and emission lines. BL Lac objects, on the other hand, exhibit very weakened emission and absorption lines in their spectra, if any are observed at all. There is a large amount of ongoing research into the difference in these radio-loud and radio-quiet spectra. As can be inferred from the name, BL Lacerate is the prototype object for this class of blazars, meaning that it was the first. These BL Lac objects can also be subdivided by where the peak of their emission is located in their spectra. These two classes are labeled low-energy peaked and high-energy peaked BL Lac objects (LBL/HBL). This peak is namely due to the synchrotron radiation coming from relativistic particles in their jets (Liu 2009). This synchrotron emission will obey a power law across the entire spectrum, being presented as a continuum. Therefore, where energies are higher, the spectrum will simply look like continuum emission.

Because blazars, and therefore BL Lacs, are oriented along our line of sight, most, if not all, of the radiation observed is from the jet. The radiation from the jet is so much more intense than that from the galaxy, that it is difficult to discern emission and absorption from within the galaxy. Furthermore, seeing as the gas near and within the jet are moving at relativistic speeds, all of the emission and absorption will be severely Doppler broadened. This broadening of spectral emission/absorption lines occurs due to the distribution of velocities of a certain cloud of material. Therefore, some of the material will be moving slower than the average, being less Doppler shifted than the average particle. This can also be said of the faster particles within this "parcel" of material. The result is that the spectral line has a width related to its velocity (Livadotis 2018). A higher velocity corresponds to a wider velocity distribution, which in turn corresponds to a broader spectral line. The material in an AGN is relativistic, so the lines will be broadened to a width large enough where they cannot be identified, or have a high enough signal-to-noise. Therefore, only string lines from within the jet or the galaxy itself can be measured.

Within this study, I will investigate the spectrum of BL Lac in order to find its redshift, determine its composition, and characterize the motion of particles near its center. This can be done using the aforementioned Doppler broadening, and fitting certain observed spectral lines, if any can be distinguished. I have obtained two sets of data from two different databases: one in the UV region of the spectrum and one in the optical. The optical range within the spectrum should produce more results than the UV range, as UV is higher energy than optical, meaning spectral lines will be broadened more significantly. Furthermore, shorter wavelengths will be dominated by the power law continuum produced by the synchrotron, nonthermal radiation of the jets (Dondi & Ghisellini 1995).

However, both the optical and UV data will be useful in determining whether this object is a HBL or LBL. If the UV spectrum produces no fruitful results in terms of characterization of the AGN or identification of spectral lines, it can be used to determined the material between the observer and the object. Seeing as most of the Universe, and the IGM is composed of Hydrogen, we would expect to see intervening Hydrogen absorption if there were any clouds of gas between us and BL Lac. The most prominent line observed in Hydrogen is the Lyman-α line, which is has a transition wavelength of 1215.67 $\mathring{A}$ (Hunstead & Mar 1995). Therefore, if Lyman-α emission is seen in the UV band, there could be material between us and BL

Lac. However, if no Lyman-α emission is seen, then either there is no Hydrogen in BL Lac, or it is at a redshift lower than the lowest wavelength recorded by the spectrum. This Lyman-α emission can therefore constrain the redshift of the object.

The paper will be organized as follows: a description of the data in both bands, a description of the reduction and analysis of the data, a a presentation of the results gotten from the data analysis, and discussion of the results and their implications on the characterization of BL Lac.

2. Description of the Data

In order to properly analyze the spectral features of BL Lac, two parts of the spectrum were obtained: one from the UV and one from the optical. The UV spectral data was obtained using the MAST[2] database, and the optical data was obtained using NASA's NED[3] database. The MAST database is a compilation of various different databases, including the Hubble Space Catalog and TESS. NED is a compilation of information on various extragalactic sources from a large number of different databases, including MAST and HEARSC. Each database entry in both databases catalog the principal investigator of the observation, the date of the observations, and publications that have referenced these observations.

The set of data centered in the UV band of the spectrum was observed from the Hubble Space Telescope with the G190H filter of the Faint Object Spectrograph. This observation had a resolution of R 1300, and were taken with exposures of 1440 seconds. These observations were requested by Angel in May of 1992. The set of data centered in the optical wavelengths, technically the H-β band, was taken from the Palomar 200 in. telescope. These observations were taken with a resolution of 9 Å, with exposures of 6035s. These observations were taken in 1996 by Lawrence et al. (1996). Note that there is a discrepancy in the times both of the observations were made. The observations in the optical were taken 4 years after the observations in the UV band. Due to this time-delay, there could be variation in the spectra overtime, given BL Lac objects are highly variable. However, this variation should only change the intensity, meaning the depth/height, of certain spectral features. These features would be highly Doppler broadened, seeing as they would be near the center of the galaxy, meaning a change in depth would not be significant in contrast with the noise. Subsequently, the lines that are most significant within the galaxy and near the jet will not vary very much overtime, let alone over four years. Therefore, this time-delay should not produce any significant discrepancies between both sets of data, though it is important to consider.

[2]https://archive.stsci.edu/

[3]https://ned.ipac.caltech.edu/

Fig. 1.— This is an example of one of the FITS files downloaded for the UV end of the spectrum. The vertical axis represents the vertical extent of the target on the sky, while the horizontal axis represents wavelength. The large feature in the center corresponds to the large spike seen in the center of the spectrum in Figure 2.

3. Data Reduction

In this section, I go into detail on how the data was reduced into a form which is more suitable for data analysis. The start of this process involves the raw data described in §3.1/3.2, and ends with data that will be used throughout §4.

3.1. UV Spectrum

The UV spectrum was downloaded as a set of FITS files, which look like Figure 1. The vertical axis of each fits file represents the vertical angular extent of the target on the sky. Therefore, the top of the FITS file represents the top of the target on the sky, while the bottom of the image corresponds to the bottom of the target. The horizontal axis corresponds to wavelengths along the grating, which in this case are in the UV part of the spectrum. In order to reduce this data into one spectrum, not multiple as presented in the FITS files, I averaged each column of pixels. This granted one row of pixels for each file, meaning one sample of data for each file. Two of the files represented the flux and error in the flux in physical units across the spectrum, which are presented in Figure 2. The other files represented the data and error in electrons and other non-physical units used by the

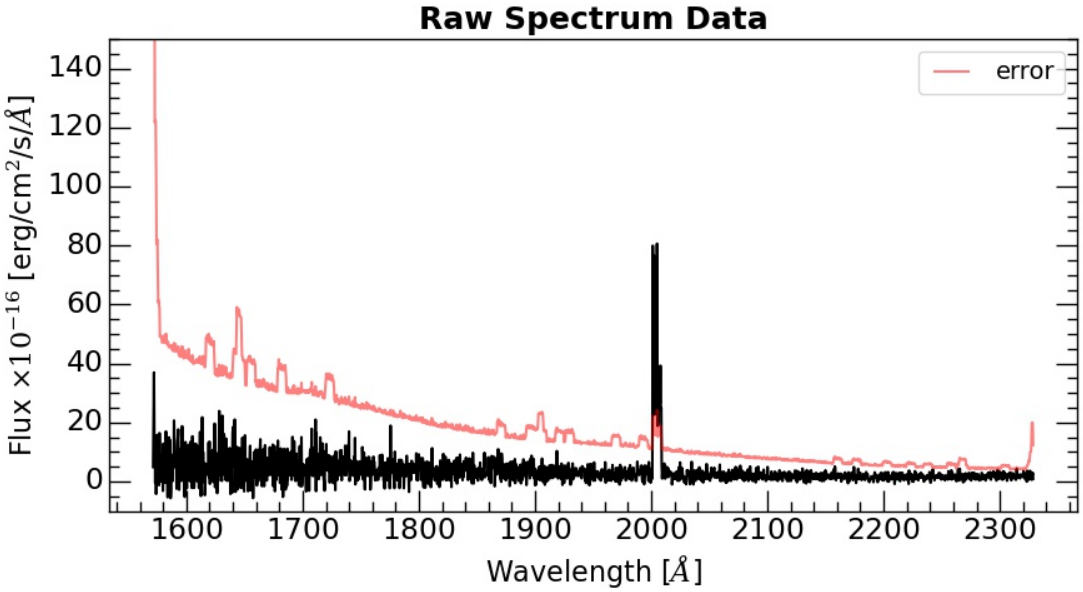

Fig. 2.— The raw data of the UV spectrum of BL Lac, given in physical units. The error is seen to be very large at shorter wavelengths, while more manageable at longer wavelengths. The large spike in the center of the spectrum is most likely not a result of emission from the target.

CCD, as well as the wavelengths used in the grating.

Simply from looking at the data, one can see that the error is very large throughout the spectrum. At the shorter wavelengths, the error in the data is almost five times the value of the data itself. There are also a large number of high amplitude variations at the shorter wavelengths, suggesting that any features discovered at shorter wavelengths are most likely noise. At the longer wavelengths, the error is much more manageable, being almost on the order of the data. However, there are no features seen on the longer end of the spectrum. The only feature seen in the UV spectrum is a sharp spike near 2000 Å. It is unclear whether this is an emission feature from the galaxy, a cosmic ray, or simply due to systematic or background noise. In order to make this feature clearer, I coadded the spectrum every two pixels. This still did not make the feature clearer, and simply increased the already large error on the data. I then convolved the data with both a boxcar function with a full-width half-maximum (FWHM) of 3, and a Gaussian with a FWHM of 1. These both produced similar results, with the Gaussian making the feature a bit clearer and smoother. Even after the convolution, the emission still does not seem to be an emission line. It does not follow a Gaussian or Lorentzian profile. Therefore, we discard this as a potential candidate for a spectral line. Even though this UV data did not produce any direct information on the location of spectral lines, and therefore the redshift or composition, it will have a notable indirect consequence in §4.3.

3.2. Optical Spectrum

The data from the optical (Hβ) band was acquired in CSV format. The only information provided was the flux in physical units corresponding to a particular wavelength. There was no error information given, so it is assumed that it was taken into account when processing this data. Seeing as this data is already processed, and fairly clear, I did not need to coadd it (Figure 3). However, in order to make the spectral features abundantly clear, and to distinguish them from noise, I convolved the data with a Gaussian with a FWHM of 1 and a boxcar function with a FWHM of 1. The data convolved with the Gaussian made the

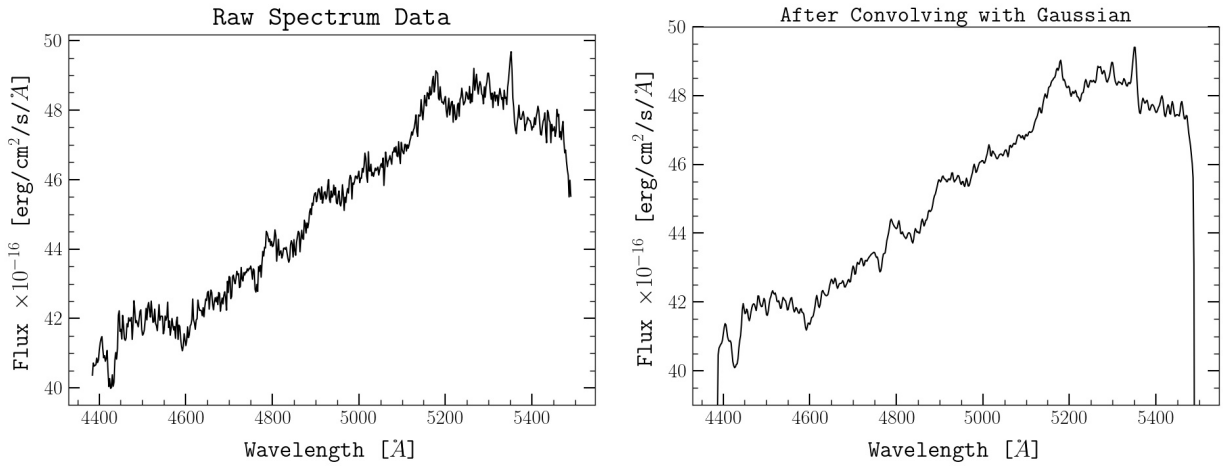

Fig. 3.— This is the raw data received for the optical section of the spectrum. Many more prominent features are seen in this part of the spectrum than in the UV. After convolving with a Gaussian (FWHM of 1), the features within the spectrum could be distinguished with even more clarity. There is a few clear peaks near 5200 Å, and a strong dip near 4400 Å.

features in the spectra much more prominent compared to the noise, while the boxcar function kept the variation from the noise. Therefore, in this study of the optical spectrum we will continue to use the data convolved with a Gaussian (Figure 3).

4. Data Analysis

The main goal in analyzing this data is to determine the material within BL Lac, its velocity with respect to the galaxy, and the object's overall redshift. Most of this data analysis will involve fitting the spectral data using least squares methods. All of these methods are provided by the `scipy` module in Python. Using these methods provides uncertainty on the values fitted for, as well as a probability for rejection, provided that there is a sufficient amount of data compared to the number of parameters being fit for.

4.1. Finding the Extrema

In terms of finding the emission and absorption lines on the spectrum, identifying lines by eye may suffice if they are pronounced enough. However, seeing as the emission and absorption from BL Lac is severely Doppler broadened, fitting for the extrema on the spectrum serves as a more statistically significant option.

Initially, I normalized the flux of the spectrum in order to make peaks in the data easier to distinguish. In order to do this, I fit the spectrum on a line using the `linregress` function in `scipy`. After fitting for the slope and intercept of the line, comparing to the data granted $\chi^2_\nu = .824$. This signals that the fit suits the data decently well, though the uncertainty is somewhat larger than the residuals given by the model. Though, with regards to identifying spectral lines, this should prove sufficient. Doing this allowed the features in the data to become much more prominent as compared to the raw, Gaussian-convolved data. This fit to a linear flux profile is simply an approximation, so there is definitely error associated with it. Normally, the spectrum of the jet in the center of an AGN obeys a power law (Dondi & Ghisellini 1995), and the spectrum of a galaxy varies by the characteristics of its stars. Figure 4 displays the normalized data.

Using the `find_peaks` function in the `scipy` module grants the acquisition of maxima throughout an array of data. The way in which this function determines peaks in the data can be altered by an input minimum height for the peak to reach, minimum threshold distance from data near the peak, minimum distance between the

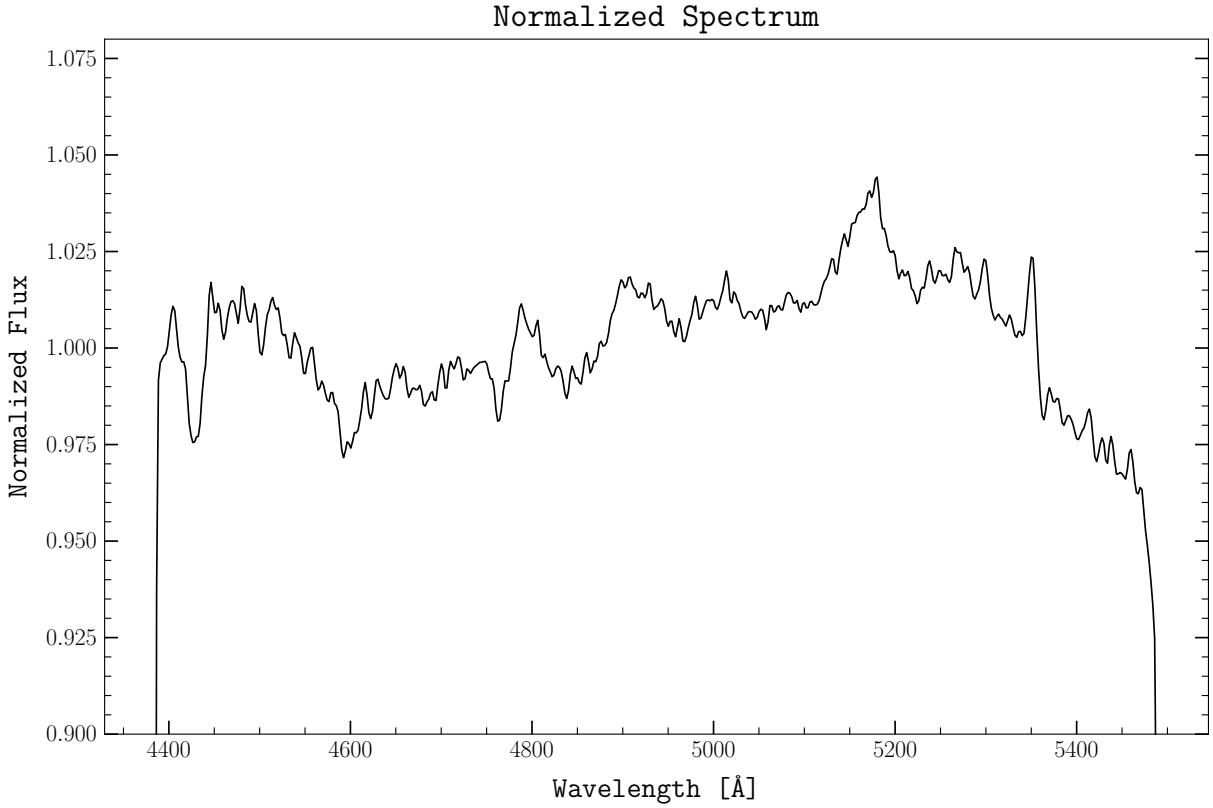

Fig. 4.— This is the normalized spectrum for BL Lac in the Optical H-β band. This was normalized by fitting a line to the spectrum, and using that as the baseline flux. Using the **scipy.optimize** module, we fitted values of $m = .00776$ and $b = 6.7491$ for the equation $y = mx + b$. This granted a $\chi^2_\nu = 429.102$, making this a reasonable approximation.

peaks, and relative prominence compared to the whole dataset. For these calculations, I had chosen a minimum distance between the peaks of 15Å, seeing as most of the large-scale, broadened features spanned tens of angstroms, and a minimum prominence of .01. This minimum prominence was found by observing the highest peak in data was about .05 greater than the mean, and the lowest was about .01 greater. To grant more peaks, as not not lose any smaller peaks, I chose a smaller minimum value for the prominence. Using this function granted a large number of peaks, on the order of 30. This function also only accounted for maxima, not minima, in the data. Therefore, I also used the `argrelmin` and `argrelmax` functions in `scipy` to find relative minima and maxima in the data. These functions only required the number of data points away from a particular maximum/minimum it would compare to. The detection of maxima proved to be much more sensitive than the detection of minima, causing me to chose a value of 12 points for the maxima function, and 17 for the minima function. This granted a lesser amount of maxima, and an even smaller amount of minima. After performing both of these filtration techniques, I then took the intersection of both datasets, and declared that the list of extremum of the spectrum.

However, I had noticed that even fairly insignificant peaks in the spectrum were being flagged as significant. Adjusting the parameters within all of the functions I had used would cause the larger peaks and dips to be left out. Subsequently, I had to filter out the smaller extrema by hand. The re-

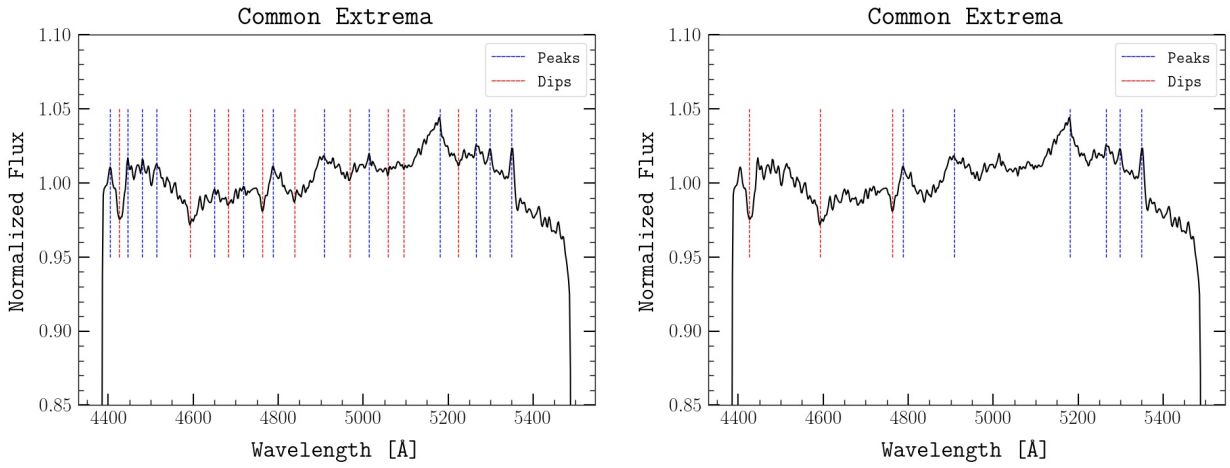

Fig. 5.— Plots of the extrema found using methods within the `scipy` Python module. After fitting for the extrema in the figure on the left, many insiginificant extrema were flagged. The resulting extrema on the right are the result of filtering the initial common extrema by hand.

sulting extrema totaled to three absorption lines and six emission lines (Figure 5).

4.2. Fitting the Extrema

After identifying the extrema across the spectrum, I then fit for the various parameters of each spectral line. Fitting for these parameters would allow me to rule out certain extrema as statistically insignificant, as well as describe certain properties of the material emitting/absorbing material in BL Lac. Again using the `scipy` module, I fit each of the spectral lines using the `curve_fit` function. This function requires an function and its parameters to minimize, as well as an input and output dataset. I fit each spectral line to a particular variation of the Gaussian function:

$$G(x) = C - D\exp\left[-\frac{1}{2}\left(\frac{x-\mu}{\sigma}\right)^2\right] \qquad (1)$$

where μ is the center of the Gaussian and σ is its standard deviation. $|D|$ is the scaling factor of the distribution, and can therefore tell us the depth of the spectral line it is fitting for. C is the baseline flux that the Gaussian will start from, in this case being the mean of the normalized flux, which is approximately 1. Fitting for σ in turn allows us to get the FWHM of the spectral line, as the FWHM of a Gaussian is $2\sqrt{\ln(2)}\sigma \approx 2.35\sigma$. The results of these fits are visualized in Figure 6. Fitting each extremum to a Lorentzian or Voigt profile may be more suited for detailing the characteristics for each spectral line, but a Gaussian is suitable to first approximation, and for the purposes of finding the redshift of BL Lac and identifying its composition.

After each spectral line was fit for, there were a few that could be removed as potential candidates. The second peak near 4900 Å could be removed, as the uncertainty in its width was too large, being almost 150 Å. The fourth peak near 5275 Å could also be removed, as its depth is significantly smaller than any of the other lines. Furthermore, many of the features due to noise are on the same order of depth. Therefore, the number of potential candidates for spectral features has been reduced to 7.

Fitting for the FWHM of each line, and its center, can then grant us a velocity of the material causing it, and possibly its temperature. The speed of material causing thermal Doppler broadening is given as:

$$v_D = \frac{\Delta\lambda}{\lambda}c = \sqrt{\frac{8\ln(2)k_BT}{m}} \qquad (2)$$

where $\Delta\lambda$ is the FWHM, λ is the peak wavelength, k_B is the Boltzmann constant, c is the

speed of light, T is the temperature of the emitting/absorbing gas, m is the mass of the particles, and v_D is the Doppler broadening velocity (Meftah et al. 2018).

4.3. Fitting the Redshifts

One of the main goals of this data analysis is to find the redshift of BL Lac. In finding the redshift, we can then find the materials located within the galaxy, or its jet, as well as the temperatures of these materials through Eqn. 2. Finding the redshift of the AGN was an overall more arduous task than fitting for the extrema or finding the Doppler broadened velocities of each spectral line. To macth certain spectral lines, I used the list of atomic transitions, and their corresponding wavelengths, in Table 3. These atomic transitions are the most prominent ones found in galactic spectra within the optical band. From the observation of the UV part of the spectrum, we can place a limit on the highest redshift possible. There was no large Lyman-α emission line seen in the UV spectrum. The large spike in the UV spectrum is most likely noise, not emission. All galaxies will have Lyman-α emission, whether it be from Hydrogen within the galaxy or Hydrogen gas intervening on our line of sight with the galaxy. Therefore, we can use the lowest wavelength measured as the highest possible redshift for the Lyman-α line. The Lyman-α line is located at near 1220 $\mathring{A}$, and the lowest wavelength recorded in the UV spectrum is near 1580 $\mathring{A}$. To find the redshift of any emission line, we can use the following formula:

$$z = \frac{\lambda_{obs} - \lambda_{em}}{\lambda_{em}} \tag{3}$$

where z is the redshift, λ_{obs} is the observed wavelength, and λ_{em} is the wavelength of the transition if it were radiated at rest in a vacuum. Using this formula, and the two wavelengths discussed previously, the largest redshift possible is .295, which I will round to .3 as a conservative estimate.

Now, again using the `curve_fit` function, I fit for the redshift of each of the spectral lines in the data, using each of the transitions in Table 3. Consequently, each line fitted to a certain transition granted a certain redshift. There are no uncertainties on the redshifts given, as there is only one parameter being fit for, and only on data point given. Therefore, in total, there were 315 redshifts produced by this method. In order to organize these redhsifts, I grouped them in intervals of .01. This granted a group of fits whose redshifts were between 0 and .01, another whose redhsifts were between .01 and .02, and so on. I filtered through these binnings of redshifts based on if they could account for the three most prominent features in the spectrum. In terms of the colloquial names I have given them, they are dip 1, peak 3, and peak 6 (Fig. 6). If these binings of redshift did not contain fits for any one, or all, of these features, I discarded them. In doing this, I found that any redshift lower than .06 could not account for the sixth peak. I also found that any redhsift above .1 could not account for the strong absorption in Dip 1. Therefore, this constrains our redshift range to $.06 < z < .1$, leaving four bins left. I display all of these bins, including the transitions and fitted redshifts, in Table 4.

After getting these fitted measurements, I then began filtering out certain bins by the compositions of the spectral lines they were fitted for. For example, in the fourth bin, the third, and largest, peak was fitted to Ar-IV. It is very unlikely that this large, broad absorption line is the fouth energy level transition of Argon, seeing as it is unlikely and therefore uncommon in most galaxies. Therefore, we can rule out the bin containing all redhsifts in the range [.09, .1]. Similarly, the bins corresponding to redshifts in the range [.07, .09] does not account for the large third peak. Therefore, we can rule out these bins. The final bin corresponds to the range $.06 < z < .07$.

5. Results

In the following few paragraphs, I describe the results obtained from the velocity measurements of all of the spectral lines. I also go into more depth in discussing which extrema from Figure 5 are actual spectral lines and which are simply features of the noise. Velocities have already been calculated via Eqn. 2 and are presented in Table 1. Possible redhsifts for the various extrema on the spectrum are found in Table 4. Some spectral lines have already been ruled out, leaving only the first set of redshifts, which is discussed in §4.3.

Table 1
Characteristics of Each Extremum

Name	λ_0	σ	FWHM	Depth/Height	v [km/s]
Dip 1	4427.80 ± .57	7.92 ± .57	18.61 ± 1.79	.034 ± .002	1261.5 ± 121.5
Dip 2	4597.49 ± .74	8.94 ± 1.07	21.00 ± 2.52	.016 ±.001	1371.8 ± 164.4
Dip 3	4763.45 ± .32	4.09 ± .43	9.60 ± 1.01	.013 ± .001	604.8 ± 63.5
Peak 1	4794.47 ± .95	12.68 ± 2.04	29.79 ± 4.80	.017 ± .002	1866.3 ± 300.8
Peak 2[a]	4919.73 ± .89	146.34 ± 449.15	···	.322 ± 1.923	···
Peak 3	5169.88 ± .69	23.15 ± 1.50	54.40 ± 3.53	.027 ± .001	3150.5 ± 204.3
Peak 4[a]	5269.06 ± .78	4.27 ± .94	···	.008 ± .001	···
Peak 5	5297.89 ± .99	3.96 ± 1.11	9.32 ± 2.60	.013 ± .003	527.5 ± 147.3
Peak 6	5349.61 ± 1.51	4.12 ± 1.56	9.69 ± 3.67	.028 ± .009	543.3 ± 206.0

[a]These two were discarded as spectral line candidates, and have no FWHM or velocity measurements

Note.—These are the characteristics determined by the **curve_fit** method in Python. The second and fourth peaks were discarded due to large width and small depth respectively. The depths/heights are given in normalized flux units.

5.1. Velocity Measurements

From Table 1 and Figure 4, we can see that most of the spectral lines are highly Doppler broadened. This follows from the fact that BL Lac is a blazar, and most of the radiation we see is coming from its relativistic jet. Four of the seven spectral lines correspond to velocities over 1000 km/s in the particles that form them. The highest velocity seen is near 3000 km/s from the large, highly broadened emission line near 5200 Å. This emission line would need to be more towards the center of the jet, being approximately .01c. The other relativistic lines either have much less material than the larger one, or are located farther away from the center of the jet. There are three other spectral features that have much lower velocities. These velocities correspond to material within the galaxy (Livadotis 2018), and are much slower in comparison to the material within the jet. These smaller spectral lines have velocities of near 550 km/s, and are most likely located either in the accretion disk near the jet, or further out in the span of the galaxy.

5.2. Further Deducing the Redshift

It is clear that the redshift lies somewhere in the range $.06 < z < .07$. We can further constrain this value by considering the transitions fitted for the different spectral lines in BL Lac. Within this range, the only fit granted for the first absorption line is $z = .0682$ for He-I. The only fit given for the fifth peak is $z = .0684$ for O-III. The large third peak is only fit to Hβ, with a value of z=.0656. These three lines are very prominent in the spectrum even before normalization, signaling that they are real. The third peak is actually asymmetric, signaling that the real redhsift of the material could be in a larger range than fitted for. Therefore, the actual redshift of BL Lac seems to be near this value of .067. Using this, we can rule out several values for the third absorption feature, and the first peak. We are then left with two redshift values for the second dip, two for the third dip, two for the first peak, and two for the sixth peak.

The emission in both the sixth and fifth peaks look very similar, being almost exactly Gaussian and very thin, suggesting that they are both in the same area of the galaxy, and/or the same type of material. The sixth peak could either be, at this point, emission from O-III or Fe-II. The first peak is known to be Fe-II, only differing by two different transitions, so we expect any spectral feature involving Fe-II to be broad and high velocity. The sixth peak is very thin, and therefore has a relatively low velocity. Therefore, we can rule out the possibility of this peak being Fe-II. Therefore, the sixth peak must be due to O-III, with a redshift of $z = .0685$, which is near the other O-III peak as well.

The third dip can be attributed to either Fe-II or He-I. We have already confirmed a very strong absorption line feature for He-I, so it is likely that

Table 2
Identified Spectral Lines

Transition	λ_{obs} [Å]	z	v [km/s]
He-I	4427.80 ± .057	.0682 ± .0001	1261.5 ± 121.5
Hβ	5180.1 ± 15	.0656 ± .0021	3150.5 ± 204.3
O-III	5297.89 ± .99	.0684 ± .0002	527.5 ± 147.3
O-III	2349.61 ± 1.51	.0685 ± .0003	543.3 ± 206.0

Note.—The final set of identified spectral lines in BL Lac. The emission due to O-III is more plausible, due to the double-peaked emission. Hβ emission is clearly broadened, and stands out against the rest of the spectrum. He-I absorption can be inferred to be highly ionized outflow from the host galaxy of BL Lac.

this could be He-I. However, the third dip is significantly slower than both the Fe-II line in the peak and the He-I line in the first dip. Therefore, we can rule out the possibility of the third dip as a spectral line, and declare it a product of noise. The second dip is either G-band absorption, or Fe-II absorption. The first peak is already considered to be Fe-II emission. This means that either the first peak is Fe-II and the second dip is G-band absorption, or the first peak is due to noise and the second dip is Fe-II absorption. Seeing how the second peak nearest to the first peak was declared a characteristic of noise, it can be declared that the first peak is noise. Furthermore, the second peak was much larger in depth than the first peak, meaning noise can vary at fluxes much larger than the first peak. Using this logic, we can declare the second dip as either G-band or Fe-II absorption.

Overall, we have confirmed a redshift for dips 1 and 2, and peaks 3, 5, and 6. Seeing as we have ruled out peak 1 as a potential spectral line, many other lines near it with similar depths/heights should also be looked into in further detail. Peak 1 has a height of .017 and dip 2 has a depth of .016. Seeing as these both are in the same region of the spectrum, have similar depths, and one of them is noise, we can declare both of them to be noise as a conservative estimate. Therefore, we have confirmed that dip 1 and peaks 3, 5, and 6 are spectral lines corresponding to He-I, Hβ and O-III. These lines grant redshift values of z = .0682, .0656, .0684, .0685 (Table 4). The value calculated by fitting the Hβ line was nearly 10 Å off from its value determined from determining extrema. Therefore, we can give a conservative uncertainty of 15Å to the wavelength for the Hβ line. Averaging these values grants a redshift of $z = .0677 \pm .001$.

6. Discussion

From the discussion in §5, we have obtained a redshift value of $z = .0685 \pm .001$, as well as identified the existence of three spectral line features and their corresponding velocities (Table 4). Each of these spectral lines and the calculated redshift will be discussed in the following sections.

6.1. He-I Absorption

My results produced the identification of He-I absorption with a redshift of .0682 and a velocity of 1261.5 km/s. This suggests that there is ionized Helium within the jet, moving at relativistic speeds, absorbing certain material as it flows through the jet. Or, this could suggest very hot and ionized Helium in the intergalactic medium. Falomo et al. (2014) state that the bulk of baryonic matter probably lies in the CGM and IGM at low redshifts. If this is the case, and the extrapolation of this data is correct, then this absorption of He-I is likely from ionized Helium in the IGM/CGM. Thre is also evidence of Helium, and Helium-like elements, serving as absorbers in AGN systems due to high-energy ionized outflows

(Pounds et al. 2003). Though these Helium absorption systems flowed at superluminal speeds, and displayed much shorter wavelength absorption features, the same principal can be applied in this situation. There could be outflows from the galaxy, or the jet, or the surrounding IGM, that is moving at relativistic speeds. This material then absorbs the emission from the jet, and is not broadened very much as a result. This observation of He-I could then signal to feedback processes in the galaxy, as well as mechanisms fueling the jet, or causing quiescence.

However, it could be the case that this absorption line is simply broadened by noise instead of by its relativistic speeds. It could also be the case that this He-I absorption is simply a large, nearby emission line feature that continues toward the shorter wavelengths. If this were the case, then this He-I absorption wouldn't be absorption at all, but the dropoff from a large emission line at wavelengths shorter than the data provides. If we assume that the ionized Helium resides within the galaxy, and not at the relativistic speeds we have calculated, Lynden-Bell (1967) suggests that BL Lac is located within a giant galaxies. Seeing as most BL Lacs are located within giant elliptical galaxies (Falomo et al. 2014), this conclusion makes sense.

Consequently, both of these different scenarios suggest that this observation of He-I is real. Either this ionized Helium is a particular outflow from the galaxy, or a strengthened absorption line from within the galaxy. Both scenarios have evidence that support their formation.

6.2. Hβ Emission

The observed spectral line of Hβ within BL Lac is highly Doppler broadened, having a velocity near 3100 km/s, with a redshift of .0656. Hβ is predicted to be in all AGN, as Hydrogen is the most ubiquitous element in the Universe, and therefore the IGM and CGM. Seeing as this line is highly broadened, it is located in the broad-emission line region (BLR) of the spectrum, as opposed to the narrow-emission line region (NLR). The NLR is characterized by a variety of narrow-emission lines, with material causing the emission traveling at a few hundreds of km/s (Osterbrock 1991). In contrast, the BLR consists of broad emission lines, with material traveling at highly relativistic, possibly even superluminous, speeds. In the spectrum of BL Lac, we can see that these regions are supermimposed on top of each other, with broad Hβ occurring near narrow O-III emission. There is much contemporary research in explaining the physical reasons for these two emission line regions in AGN spectra, but is outside the scope of this paper. It is also known that within AGN, this broad Hβ line stems almost entirely from recombination (Baskin & Laor 2005). The Hydrogen falling into the black hole at the center of the galaxy will be accelerated to such high speeds in such a compact region that recombination and photoionization will begin to occur. This releases a large amount of radiation towards the center of the galaxy, as the gas is extremely ionized. Thus, the Hβ line is an indicator of the characteristics of the black hole, and the mechanisms powering the jet.

It can also be seen that the Hβ line from BL Lac is asymmetric, leaning slightly towards the longer wavelengths. There are multiple explanations for why the Hβ emission line would be asymmetric towards lower energies, as this is not just a property of BL Lac. Boroson & Green (1992) suggest that this "asymmetry" is actually due to abundances in Fe-II. There is notably a strong correlation between Fe-II abundance and this Hβ asymmetry. It has also been shown that this Hβ asymmetry correlates to the luminosity of O-III emission (Czerny 2019). Seeing as there is observed O-III emission in BL Lac, this Hβ emission serves as a piece of suggestive evidence. This relation to Fe-II and O-III abundances involve relativistic effects, such as the time lag from different part of the clouds of gas emitting material at high speeds, as well as the column density of the cloud along our line of sight. Therefore, if we are to take this correlation between O-III abundance and Hβ symmetry to be fact, then the existence of both of these features in BL Lac makes physical sense.

Overall, it is well known that Hβ will be present in most, if not all AGN, and will be part of the BLR.

6.3. O-III Emission

We have calculated that there are two, narrow emission lines corresponding to O-III, with their rest wavelengths of 4598.91 Å and 5006.84 Å. These emission lines both have respective veloci-

ties of 527.5 km/s and 543.3 km/s. These emission lines both fit the requirement of fitting into the NLR of AGN spectra. Furthermore, the NLR contains various forbidden emissions, while the BLR only contains permitted emissions. Forbidden emissions, such as O-III, are atomic transitions that are extremely weak, and cannot be reproduced on Earth. These transitions are highly improbable and can only be reproduced in a very low-density medium, such as within a galaxy. Therefore, forbidden emissions should be narrower than permitted emissions, seeing how they are much less probable, and therefore should occur less often. The fact that these lines are narrow also signals that they are further out from the galactic center than lines in the BLR. These lines are not as broadened as lines in the BLR, such as Hβ, so they would be in a less-dense environment further from the black hole at the galactic center (Richardson et al. 2014).

It is known that O-III emission is produced more so from collisions between atoms than thermal absorption and re-radiation (Baskin & Laor 2005). Therefore, O-III can act as an indicator of the density of material within a galaxy. It is also known that O-III is present in almost all AGN, and can be an indicator of a galaxy being an AGN. Galaxies with a higher ratio of [O-III]5007$\AA$/Hβ are AGN, while those with a lower ratio are star-forming galaxies (Suzuki et al. 2016), (Baldwin et al. 1981). Furthermore, there is evidence that BL Lac objects have significantly higher O-III luminosities than extended, low-power radio galaxies (Wills et al. 2004).

Therefore, the presence of O-III in BL Lac is expected, especially within the NLR in the optical spectrum. This serves as an indicator for the type of galaxy it is in, a massive elliptical, and the density of gas farther from the galactic center.

6.4. Redshift and Spectrum Characteristics

The redshift gotten from the fitting of data suggests that BL Lac is relatively close to our galaxy. This also suggests that there should not be very much material in the IGM or CGM along our line of sight. As seen from the UV part of the spectrum, there are no features signaling Lyman-α absorption, which is the largest indicator of intervening IGM gas. Therefore, this value of redshift is somewhat supported. There was absorption seen from He-I, though this is most likely due to ionized outflow of the galaxy, not material in the IGM at a lower redshift. The redshift of the He-I absorption is also within the uncertainty of the redshift of the entire galaxy, meaning it would be highly unlikely that it is at a lower redshift.

Additionally, we can characterize this spectrum as being a QSO (quasi-stellar object), as the BLR almost completely overpowers the NLR. This occurs because most of the radiation observed is coming from the jet and accretion disk, not the stars within the galaxy. It can also be seen that this spectrum peaks in the optical, or at longer wavelengths. Therefore, this object can be classified as an LBL. The lack of features in the UV band also substantiate the fact that this is a blazar, as no high-energy spectral lines are observed, being overpowered by jet radiation.

7. Comparison and Conclusion

The results of this investigation are substantial, despite the fact that most BL Lac spectra are featureless. Using the `scipy` package within Python, I have reduced and analyzed two parts of the spectra for BL Lac. This involved normalizing the flux for each set of data, and fitting the extrema in the optical band. This then required filtering the extrema while also fitting for the redshift of the entire system. After much deduction, we were left with He-I absorption, and Hβ and O-III emission. He-I emission is most likely due to ionized, relativistic outflows from the galaxy. O-III and Hβ emission are both known to be prevalent in AGN spectra, each providing insight on several characteristics within the AGN. The velocities of these broad emissions, therefore within the BLR, suggest that the jet within BL Lac is relativistic, with the Hβ line having a velocity of nearly 3000 km/s. The asymmetry in the Hβ line can be due to various factors, but two that seem reasonable in this scenario is the abundance of O-III and the time-lag in emission of highly relativistic gas near the center of the galaxy.

Comparing to results left by Vermeulen et al. (1995) for BL Lac, we can see that the spectral lines identified match. In their work, within Figure 3, one can see broad Hβ absorption, albeit more mild than in this selected sample of data,

and strong, narrow O-III emission. There is no evidence for He-I emission in their spectra, and this is only one year before the dataset I have chosen to use. Therefore, this "identification" of He-I is likely noise, though it is significant enough to flag as a feature of interest. Furthermore, the spectrum they have displayed shows a significant O-III emission line, while the emission line in the data from Lawrence et al. (1996) has a much smaller depth. This could be due to the variation of BL Lac, as it can vary on short timescales, but this is highly unlikely due to the fact that these were observed in the same year. The fact that this O-III emission is much less significant is most likely a product of the noise of the system, and the seeing at the time of observation. Both were taken from 200 in. telescopes on the ground, meaning they should have produced similar results. However, the fact that Hβ and O-III were identified shows that this reduction of data was at least a partial success.

Furthermore, their data shows similar values in the velocities of each of the identified lines to the ones I have extrapolated. For Hβ, Vermeulen et al. (1995) states that the velocity is near 4400 km/s. This is approximately 1000 km/s off from my calculated value, even with uncertainty, but both still display that the material producing the emission is relativistic. For O-III, they declare that the emission is near 500 km/s, which falls well within the uncertainty of my calculated value. Therefore, the characterization of O-III I have done in BL Lac was successful. Additionally, Vermeulen et al. (1995) produce a value of $z = .0686 \pm .004$ for the redshift of BL Lacertae, which falls within our redshift of $z = .0677 \pm .001$. Albeit, the uncertainty on the redshift is somewhat high, but solely due to the uncertainty on the central wavelength of the Hβ emission due to its asymmetry. With more sophisticated fits to the emission, accounting for the asymmetry, this uncertainty could be decreased. However, this still shows that my assumptions in determining the redshift were correct, if not somewhat successful.

Through the analysis done on both the UV and optical spectrum, I was able to successfully identify three spectral lines, obtain their respective velocities, and calculate the redshift of BL Lac. These emission lines help further characterize its properties, and allow for further explorations of the mechanisms that lead to its highly variable emission.

REFERENCES

Baldwin, J. A., Phillips, M. M., & Terlevich, R. 1981, PASP, 93, 5. doi:10.1086/130766

Baskin, A. and Laor A., 2005, MNRAS, 538, 3, 1043-1054

Boroson, T.A., Green, R.F., 1992, ApJ Supplement, 80, 109

Czerny, B., 2019, Open Astron., 28, 200-212

Dondi, L. & Ghisellini, G. 1995, MNRAS, 273, 583. doi:10.1093/mnras/273.3.583

Falomo, R., Pian, E., and Treves, A., 2014, The Astronomy and Astrophysics Review, 22

Hunstead R. W. and Mar, D.P., 1995, J. Astrophys. Astr., 16, 103-110

Lawrence, C. R., Zucker, J. R., Readhead, A. C. S., Unwin, S. C., Pearson, T. J., and Xu, W, 1996, The ApJ Supplement Series, 107, 541

Liu, X., 2009, Astrophysics and Technology ASP Conference Series, 402

Livadiotis, G., 2018, ApJS, 239, 25

Lynden-Bell, D., 1967, The Observatory, 87, 163-168

Meftah, T.M., Gossa, H., Touati, K.A., Chenini, K., and Naam, A., 2018, Atoms, 6, 16

Osterbrock, D.E., 1991, Re. Prog. Phys., 54, 579-633

Pounds, K.A., Reeves, J.N., King, A.R., Page, K.L., O'Brien, P.T., and Turner, M.J.L, 2003, MNRAS, 345, 705

Ralchenko, Y., Kramida, A.E., Reader, J. and NIST ASD Team (2010). NIST Atomic Spectra Database (version 4.0), [Online]. Available: http://physics.nist.gov/asd [Wednesday, 9-Dec-2020 6:00:02 EDT]. National Institute of Standards and Technology, Gaithersburg, MD.

Richardson, C.T., Allen, J.T. Baldwin, J.A., Hewett, P.C., and Ferland, G.J., 2014, MNRAS, 437, 3, 21

Suzuki, T. L., Kodama, T., Sobral, D., et al. 2016, MNRAS, 462, 181. doi:10.1093/mnras/stw1655

Vermeulen, R. C., Ogle, P. M., Tran, H. D., et al. 1995, ApJ, 452, L5. doi:10.1086/309716

Villata, M., 2002, A&A, 390, 407-421

K. A. Wills, R. Morganti, C. N. Tadhunter, T. G. Robinson, and M. Villar-Martin, 2004, MNRAS, 347, 3, 771-786

This 2-column preprint was prepared with the AAS LaTeX macros v5.0.

A. Fitting the Extrema

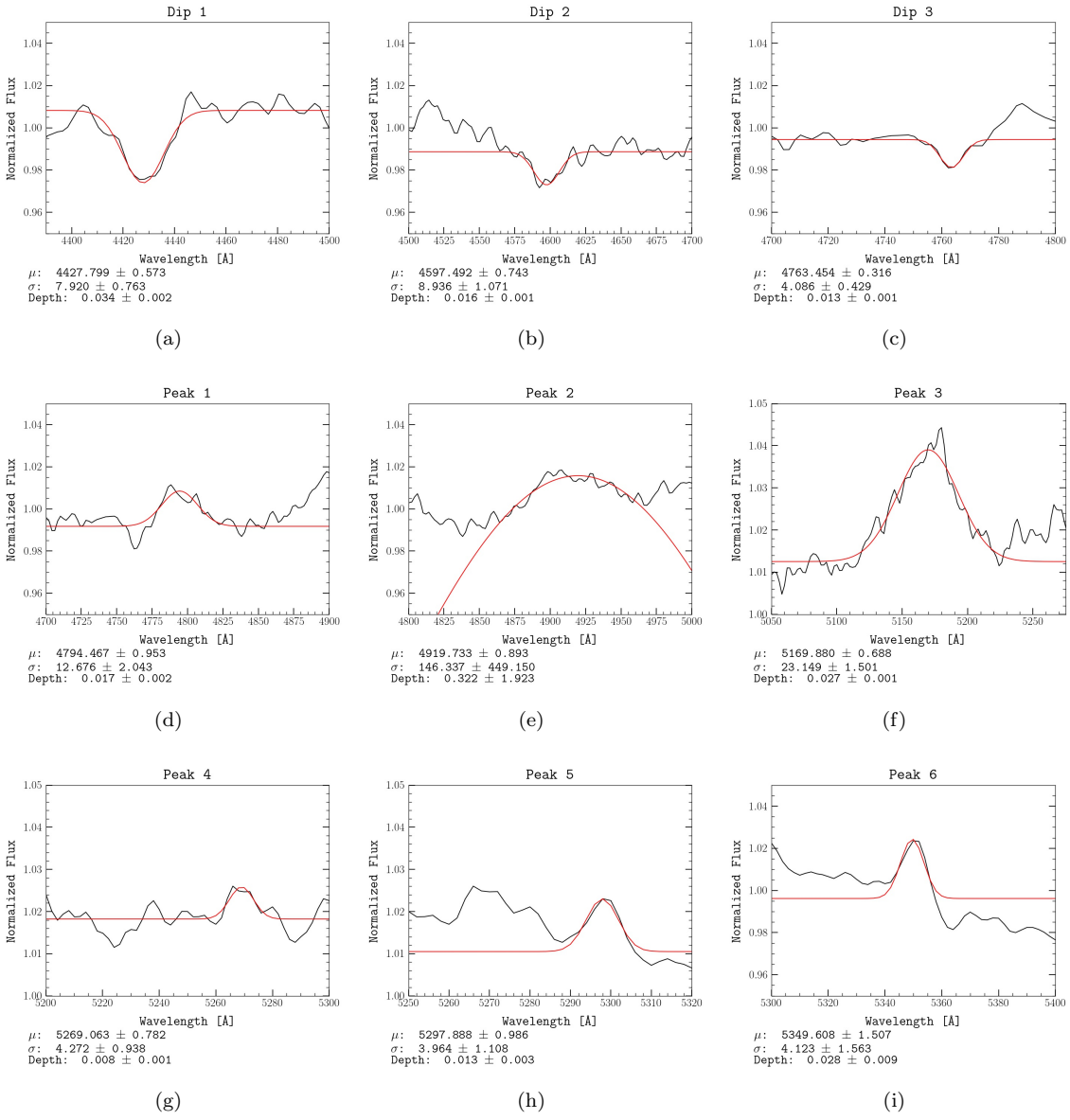

Fig. 6.— Fitting for each of the common extrema from Fig. 3. Each Gaussian fit gave a value for the central wavelength (μ), the width of the fit (σ), and the depth/height of the line. This was performed using the **scipy.optimize** module, granting uncertainties on these values as well. From the lack of depth on Peak 4, we can rule it out as an emission line. From the large uncertainty on Peak 2, we can rule it out as an emission line.

Table 3
Optical Spectral Lines

Wavelength [Å]	Transition
4026.190	He-I
4068.600	S-II
4071.240	Fe-V
4076.349	S-II
4101.742	Hδ
4143.761	He-I
4178.862	Fe-II
4180.600	Fe-V
4227.190	Fe-V
4233.172	Fe-II
4287.394	Fe-II
4303.176	Fe-II
4305.61	G
4317.139	O-II
4340.471	Hγ
4363.210	O-III
4414.899	O-II
4416.830	Fe-II
4452.098	Fe-II
4471.479	He-I
4489.183	Fe-II
4491.405	Fe-II
4510.910	N-III
4522.634	Fe-II
4555.893	Fe-II
4582.835	Fe-II
4583.837	Fe-II
4629.339	Fe-II
4634.140	N-III
4640.640	N-III
4641.850	N-III
4647.420	C-III
4650.250	C-III
4651.470	C-III
4658.050	Fe-III
4685.710	He-II
4711.260	Ar-IV
4740.120	Ar-IV
4861.333	Hβ
4903.070	Fe-IV
4923.927	Fe-II
4958.911	O-III
5006.843	O-III
5018.440	Fe-II

References.—Ralchenko et al. (2010)

TABLE 4
FITTED REDSHIFTS

Line Name	z	Transition	λ [Å]	v [km/s]
Dip 1	0.0682	He-I	4143.76	1261.5
Dip 2	0.0672	Fe-II	4303.18	1371.8
Dip 2	0.0666	G	4305.61	1371.8
Dip 3	0.0697	Fe-II	4452.10	604.8
Dip 3	0.0650	He-I	4471.48	604.8
Dip 3	0.0608	Fe-II	4489.18	604.8
Peak 1	0.0666	Fe-II	4489.18	1866.3
Dip 3	0.0603	Fe-II	4491.40	604.8
Peak 1	0.0661	Fe-II	4491.40	1866.3
Peak 1	0.0615	N-III	4510.91	1866.3
Peak 3	0.0656	Hβ	4861.33	3150.5
Peak 5	0.0684	O-III	4958.91	527.5
Peak 6	0.0685	O-III	5006.84	543.3
Peak 6	0.0661	Fe-II	5018.44	543.3
Dip 1	0.0792	Hδ	4101.74	1261.5
Dip 2	0.0711	Fe-II	4287.39	1371.8
Dip 3	0.0787	O-II	4414.90	604.8
Dip 3	0.0782	Fe-II	4416.83	604.8
Peak 1	0.0755	Fe-II	4452.10	1866.3
Peak 1	0.0709	He-I	4471.48	1866.3
Peak 5	0.0760	Fe-II	4923.93	527.5
Peak 6	0.0789	O-III	4958.91	543.3
Dip 1	0.0879	S-II	4068.60	1261.5
Dip 1	0.0872	Fe-V	4071.24	1261.5
Dip 1	0.0859	S-II	4076.35	1261.5
Dip 2	0.0864	Fe-V	4227.19	1371.8
Dip 2	0.0849	Fe-II	4233.17	1371.8
Peak 1	0.0846	O-II	4414.90	1866.3
Peak 1	0.0841	Fe-II	4416.83	1866.3
Peak 5	0.0898	Hβ	4861.33	527.5
Peak 5	0.0805	Fe-IV	4903.07	527.5
Peak 6	0.0865	Fe-II	4923.93	543.3
Dip 1	0.0994	He-I	4026.19	1261.5
Dip 2	0.0990	Fe-II	4178.86	1371.8
Dip 2	0.0985	Fe-V	4180.60	1371.8
Dip 3	0.0972	Hγ	4340.47	604.8
Dip 3	0.0915	O-III	4363.21	604.8
Peak 1	0.0974	O-III	4363.21	1866.3
Peak 3	0.0995	Ar-IV	4711.26	3150.5
Peak 3	0.0928	Ar-IV	4740.12	3150.5
Peak 6	0.0912	Fe-IV	4903.07	543.3